Characterization of the interface dipole at the paraphenylenediamine-nickel interface: A joint theoretical and experimental study

L. Lindell, M. P. de Jong, and W. Osikowicz
Department of Physics, IFM, Linköping University, S-58183 Linköping, Sweden

R. Lazzaroni
Service de Chimie des Matériaux Nouveaux, Université de Mons-Hainaut, Place du Parc 20, B-7000 Mons, Belgium

M. Berggren
Department of Science and Technology, Campus Norrköping, Linköping University, S-60174 Norrköping, Sweden

W. R. Salaneck
Department of Physics, IFM, Linköping University, S-58183 Linköping, Sweden

X. Crispin[a)]
Department of Science and Technology, Campus Norrköping, Linköping University, S-60174 Norrköping, Sweden

(Received 9 September 2003; accepted 2 December 2004; published online 18 February 2005)

In organic-based (opto)electronic devices, charge injection into conjugated materials is governed to a large extent by the metal-organic interface dipole. Controlling the injection of charges requires a better understanding of the fundamental origin of the interface dipole. In this context, photoelectron spectroscopies and density functional theory calculations are used to investigate the interaction between *para*-phenylenediamine (PPDA), an electron donor, and a polycrystalline nickel surface. The interface dipole formed upon chemisorption of one PPDA monolayer strongly modifies the work function of the nickel surface from 5.10 to 3.55 eV. The work function decrease of 1.55 eV is explained by the electron-donor character of PPDA and the modification of the electronic density at the metal surface. PPDA monolayers are composed of tilted molecules interacting via the nitrogen lone-pair and PPDA molecules chemisorbed parallel to the surface via their π-electron density. Annealing the monolayer leads to dehydrogenation of PPDA activated by the nickel surface, as found for other amines. © *2005 American Institute of Physics*. [DOI: 10.1063/1.1851507]

I. INTRODUCTION

In the field of organic-based (opto)electronics, increasing attention is being paid to the charge injection process at interfaces between the metal electrodes and the active molecular or polymeric layers.[1,2] Interfacial properties are known to significantly influence device performance.[3] For example, the efficiency of organic light-emitting diodes has been demonstrated to be directly related to the charge injection process between the metal electrodes and the organic materials.[4–6]

A simple approach to estimate the electron (hole) injection barrier for molecular materials vapor-deposited onto clean metal surfaces is to consider the energy difference between the metal work function and the lowest unoccupied molecular orbital (LUMO) [highest occupied molecular orbital (HOMO)] of the active organic material. Numerous photoelectron studies and Kelvin probe measurements[7] have demonstrated that the actual situation is more complex, since an interface dipole D_{int} can appear at the metal/organic interface which modifies the charge injection barrier.[8–12] The metal work function change ΔW upon monolayer adsorption is a measure of this interface dipole. Although there are various possible origins for the dipole eD_{int},[9] it generally consists mainly of the following three contributions:[13,14] (i) the reduction of the metal surface electron density tail upon adsorption,[15,16] which always decreases the metal surface dipole potential $e\Delta D_{met}$, (ii) the intrinsic dipole moment D_{mol} of the adsorbed molecule, and (iii) the chemical dipole potential eD_{chem} created by partial electron transfer between the metal and the adsorbate upon chemisorption.[17,18] Therefore, ΔW can be written as a function of these contributions:

$$\Delta W = eD_{int} = f(e\Delta D_{met}, eD_{mol}, eD_{chem}). \tag{1}$$

An interface dipole with its positive pole pointing towards the organic layer and its negative pole towards the metal decreases the metal work function. It also lowers the LUMO in the organic layer, with respect to the Fermi energy in the metal, by adding an electrostatic energy. As a result, the electron injection barrier ϕ_e is reduced, as illustrated in Fig. 1. Reversing the interface dipole leads to a reduction of the hole injection barrier ϕ_h. Thus, a work function decrease (increase) is associated with an improvement of electron (hole) injection. For molecules possessing a large dipole mo-

[a)]Author to whom correspondence should be addressed. Fax: +46-11-36 34 85. Electronic mail: xavcr@itn.liu.se

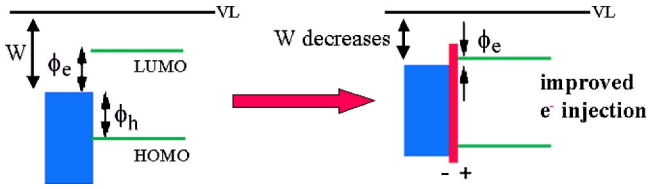

FIG. 1. Sketch of the influence of the formation of an interface dipole on the electronic levels at an organic semiconductor/metal interface. A simple approach to estimate the hole (electron) injection barrier is to take the difference between the metal work function and the highest occupied molecular orbital (HOMO) [lowest unoccupied molecular orbital (LUMO)] of the conjugated material. The hole [electron] injection barrier $\phi_h[\phi_e]$ is modified upon introducing the interface dipole.

ment oriented perpendicular to the metal surface, it has been demonstrated that the total interface dipole could be tuned by chemically changing D_{mol}.[19–22]

The aim of this work is to investigate, using photoelectron spectroscopy and quantum chemical calculations, the interaction of an electron donor, *para*-phenylenediamine (PPDA) (of which the chemical structure is shown in Fig. 2), with a prototypical metal surface (polycrystalline nickel) and to measure the direction and amplitude of the work function change upon adsorption. The adsorption of PPDA on Ni is expected to result in a large chemical dipole D_{chem} due to its electron donating character, which would in turn lead to a decrease in the nickel work function.[13] Recently, pyridine has been shown to decrease the work function of the W(110) surface by 1.9 eV.[23] Note that a possible difficulty to investigate the origin of metal work function modification upon adsorption of PPDA is the fact that amine-containing molecules undergo dehydrogenation activated by their interaction with nickel surfaces.[24–27] Hence, to be able to reach valuable conclusions on the interface dipole upon molecular adsorption, it is important to determine the temperature range at which dehydrogenation occurs.

In the first part of the paper, we present density functional theory (DFT) based models of the adsorption of PPDA on a 16-atom nickel cluster representing one adsorption site on the Ni(100) surface. In the second part, the theoretical results are compared to x-ray and ultraviolet photoelectron spectroscopies (XPS and UPS) data characterizing PPDA molecules adsorbed on polycrystalline nickel. In the last section, dehydrogenation of PPDA on nickel is discussed.

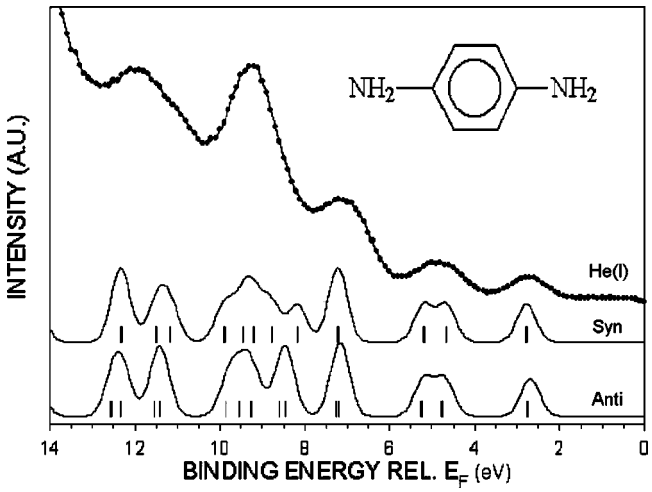

FIG. 2. Comparison between the UPS spectrum of a PPDA multilayer and the simulated spectrum for the *syn*- and the *anti*-isomers obtained by quantum mechanics calculations based on DFT.

II. EXPERIMENT

XPS and UPS were carried out using a custom-built ultrahigh vacuum (UHV) photoelectron spectrometer (base pressure $<1\times10^{-9}$ mbar). The system is equipped with a He discharge lamp and a monochromator. The resolution is ±0.1 eV, determined from the width of the Fermi edge of Au. The x-ray source produces unfiltered Al($K\alpha$) radiation at 1486.6 eV. The electron energy analyzer was operated under such conditions that the Au($4f_{7/2}$) line would be recorded with a full width at half maximum (FWHM) of 1.3 eV. With this spectrometer, all XPS spectra have been recorded with an electron emission angle of 30° defined with respect to the surface normal. Additional XPS measurements were performed using a Scienta ESCA 200 spectrometer[28] (base pressure 1×10^{-10} mbar). The ESCA 200 uses monochromatized Al($K\alpha$) radiation ($h\nu$=1486.6 eV). The experimental conditions are such that the FWHM of the gold, Au($4f_{7/2}$), line is 0.65 eV.

Atomically clean polycrystalline Ni surfaces were prepared by ion etching in the preparation chamber of the spectrometer (base pressure 10^{-10} mbar). PPDA multilayer films were deposited in UHV by exposing the Ni surface, at −85 °C, to the PPDA vapor that was leaked into the preparation chamber by means of a doser. In order to avoid any possible surface charging during UPS/XPS measurements, the thickness of the condensed multilayer films was kept well below 100 Å, as estimated from the attenuation of Ni XPS lines. PPDA monolayers were prepared by adsorption of gaseous PPDA molecules on the Ni substrate cooled at −40 °C, just above the desorption temperature of PDDA multilayers. At this temperature, the sticking coefficient was about optimal, while multilayer formation was inhibited.

III. THEORETICAL APPROACH

A. Model

Since chemisorption is a localized interaction, metal clusters can be used as models of the adsorption site on the metal surface. Two-layer clusters composed of 16 atoms are used to model the (100) surface, with interatomic distances fixed at the bulk values (see Fig. 3). The distance between the central atoms of the upper layer and the other atoms is 2.49 Å. The (100) surface is chosen because it has a surface atomic density intermediate between that of the compact (111) surface and that of the open (110) surface. Since the reactivity of the surface depends on the surface atomic density,[29] the (100) surface can be considered as possessing an average reactivity of different faces of the polycrystalline metal surface.

The choice of small clusters to model metal surfaces needs justification since numerous studies have shown that the chemisorption energy of an adsorbate interacting with metal clusters oscillates with cluster size, cluster shape, and adsorption site on the cluster. The magnitude of these oscil-

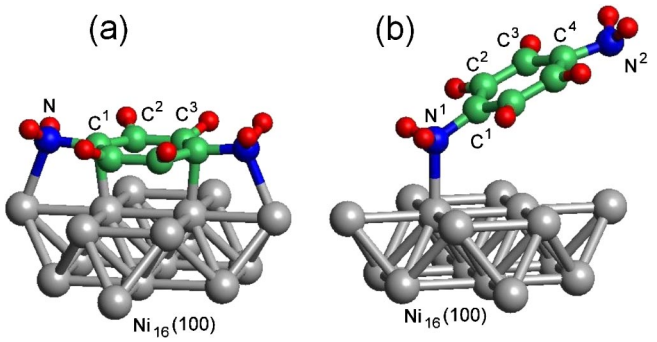

FIG. 3. Sketch of the optimized structures obtained for the two adsorption conformations of *p*-phenylnenediamine interacting with the metal surface site $Ni_{16}(100)$: (a) *f*-PPDA parallel to the nickel surface, and (b) *t*-PPDA tilted on the surface.

lations can be dramatic for (i) adsorbates interacting with the cluster via a single site, i.e., a single bond; and (ii) small quasispherical metal clusters. For CO on Cu_n (Refs. 30 and 31) [Ni_n (Ref. 32)] clusters, the chemisorption energy can change nonmonotonically by 20 kcal/mol (40 kcal/mol) with cluster size. These oscillations arise from the discrete electronic configuration of finite metal clusters:[33] the nature of frontier orbitals changes with size, so their shape in different clusters can be either more or less favorable for chemisorption. However, the chemisorption energy oscillations versus cluster size are significantly damped for (i) relatively large, π-conjugated molecular adsorbates interacting with the metal cluster via several moieties, i.e., several chemical bonds; and (ii) large and flat metal clusters. This is the case for PPDA interacting with two-layer nickel clusters: $Ni_{16}(100)$. For another conjugated molecule, acrylonitrile, the evolution of the binding energy with cluster size displays rather weak oscillations with a magnitude of ca. 8 kcal/mol.[18] The reason of this behavior is well understood. First, the use of large and flat metal clusters, rather than small and quasispherical ones, provides a metal electronic structure free of the electronic shell structure and close to the density of states of the actual metal surface.[34] Second, the presence of several (rather than one) interaction sites for the molecule on the clusters is also likely to damp the oscillations. In addition, the geometry of the conjugated molecule is not expected to depend significantly on the size of the metal clusters.[18] Therefore, the 16-atom flat nickel cluster, $Ni_{16}(100)$, appears as a reasonable model for PPDA adsorption on polycrystalline nickel surfaces.

When using cluster-adsorbate complexes with relatively large adsorbates as in this study, various aspects need to be stressed. *P*-phenylenediamine possesses several chemical groups likely to interact with the metal surface. The number of possible positions on the surface is subsequently higher than with an adsorbate interacting with only one site (such as on-top CO). Consequently, there are different adsorption geometries corresponding to local minima of the Born–Oppenheimer potential surface. The adsorption of ethylene on Ni(100) has been previously modeled using $Ni_{16}(100)$ cluster calculations.[35,36] Four different adsorption positions of ethylene on $Ni_{16}(100)$ yield similar stabilities as well as similar geometrical structures for the adsorbate, indicating a relative flat Born–Oppenheimer potential surface. Therefore, no dramatic changes in chemisorption energies and adsorbate structure are expected when a larger adsorbate, i.e., PPDA, is placed at different positions on the surface, provided that its π-bonds interact via the four positions that were identified for the ethylene case. A complete geometry optimization of a large adsorbate interacting via several of its atoms with $Ni_{16}(100)$ is thus expected to provide a good model to evaluate the structure and relative binding energy of PPDA chemisorbed in different conformations.

B. Methodology

Transition metal clusters can be accurately described by means of quantum-mechanical methods based on density functional theory.[37] These methods include a significant part of the electron correlation energy, which is essential for a correct description of transition metal compounds. The DFT calculations were performed with the DMOL program.[38,39] The chosen basis set is DNP (double ζ numeric with polarization). The core orbitals are frozen during the self-consistent field (SCF) iterations and a medium mesh size is used for the calculations.[38,39] Geometry optimizations are carried out with the eigenvector-following algorithm by Baker,[40] within the gradient-corrected approximation (using both the gradient-corrected exchange potential by Becke[41] and the gradient-corrected correlation potential by Perdew and Wang[42]). This algorithm was improved to optimize the geometry in Cartesian coordinates[43] and to introduce constraints (fixed atoms) in Cartesian coordinates thanks to an efficient Lagrange multiplier algorithm.[44] The geometry optimizations are unconstrained except for the distances between metal atoms that are kept at the bulk crystal values. The starting geometry of PPDA is flat or perpendicular on the surface of the cluster. This theoretical method is known to provide reliable adsorption geometries for molecular adsorbates.[45,46] In order to characterize the partial charge transfer upon chemisorption, the Hirshfeld partition scheme of the electronic density in atomic charges is used.[47,48] In order to discuss the bonding configuration of PPDA on nickel, the local density of states (LDOS) defined according to the decomposition scheme by Löwdin[49] is used.

After geometry optimization of the complex, with the nickel cluster structure kept fixed, the chemisorption energy E_{chem} is evaluated as the difference between the total energy of the complex and the sum of the total energies of the two isolated parts (the organic molecule and the nickel cluster). The absolute value of the chemisorption energy of a molecule on a metal surface from cluster calculations is not straightforward to obtain.[33] Our calculation of the chemisorption energy of PPDA on a nickel cluster is not aimed at determining the absolute values, but rather at estimating which adsorption geometry is the most stable, and establishing a relative scale of interaction energy.

Note that the SCF procedure used to minimize the ground-state energy shows strong oscillations in electron density and total energy. This oscillation problem is well known in systems having a vanishing HOMO-LUMO gap due to the symmetry of the system or to *d*-molecular orbitals

very close to each other in energy, as can be the case in transition metal clusters. In order to overcome this difficulty, the method proposed by Rabuck *et al.*[50] is followed: to reach convergence, one allows molecular orbitals to be fractionally occupied. Here, the valence electrons are spread over an energy window, i.e., a range of molecular orbital energies broader than that given by a Fermi–Dirac distribution at 0 K. The calculations are then performed in several steps, starting with a large energy window. At each step, the SCF convergence is reached; then, the size of the window is reduced. Finally, the last step corresponds to zero temperature and gives integer orbital occupations at convergence.

IV. THEORETICAL RESULTS

A. Valence levels of PPDA

Figure 2 displays the theoretical UPS spectrum of the PPDA molecule (both *syn*- and *anti*-isomers) and a comparison with the experimental valence level spectra of a PPDA multilayer deposited on nickel. The N–H bonds on both amine groups are on the same side of the molecular plane for the *syn*-isomer, and on opposite sides for the *anti*-isomer. The general procedure used to calculate the UPS spectrum has been described in detail elsewhere.[51] In short, this procedure can be described as follows. We simulate the spectrum within the Koopmans' approximation (i.e., using eigenvalues as binding energies), without estimating cross sections. A Gaussian function is centered (width 0.3 eV) at each eigenvalue to account for spectral broadening. HOMO of the single molecule is matched to the first ionization potential in the experimental spectrum in order to account for solid-state polarization effects. The energy scale has been stretched by a factor of 1.03 to compensate for the neglect of intramolecular electronic relaxation and change in correlation energy upon photoemission. The *anti*-conformation is slightly more stable than the *syn*-isomer (4.28 meV). Using a Boltzmann distribution to calculate the population of the two conformations, the *syn*- and the *anti*-isomers are expected to be present in approximately the same quantities at the temperature considered (−85 °C). The *syn*-isomer is found to have a small dipole moment, which is in agreement with previous experiments.[52]

The UPS spectrum of the PPDA multilayer shows seven peaks at 2.7, 4.6, 5.0, 7.1, 9.2, 11.0, and 12.0 eV relative to the Fermi level, which are well reproduced by the theoretical simulation. A comparison of the calculated UPS spectrum for the two isomers does not show any significant difference. The multilayer and simulated UPS spectra also agree well with gas phase UPS.[53] To compare gas- and solid-phase UPS, the energy reference level has to be equivalent. Therefore, the binding energy scale of the UPS multilayer is referred to the vacuum level by adding the work function of the samples (ϕ=3.8 eV). The four first peaks in the UPS simulation of the multilayer are located at 6.4, 8.5, 9.0, and 11.0 eV relative to the vacuum level; while in the gas phase, they appear at 7.61, 9.48, 10.07, and 11.9 eV.[53] The energy difference between the gas-phase and solid-phase UPS spectra gives an estimate for the intermolecular relaxation energy or polarization energy E_{pol} of PPDA.[17,54] Although small differences appear between individual peaks (the shape of the valence-hole is not identical), the mean value of the polarization energy is 1.04 eV, i.e., of the same order of magnitude as estimated for other organic compounds.[55,56]

TABLE I. Valence levels of PPDA. The first column gives the measured UPS He(I) peak binding energies in eV (relative to the Fermi level) for a PPDA multilayer deposited on Ni. The second column contains the calculated DFT energies for the *syn*-isomer. The shape of the orbitals is depicted from two different viewpoints.

UPS	DFT	Character	Top view	Side view
2.7	2.78 (HOMO)	π (C-C, n)	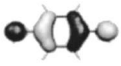	
4.6	4.66 (HOMO-1)	π (C-C)	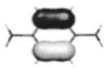	
5.0	5.20 (HOMO-2)	π (C-C, n)	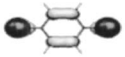	
7.1	7.21 (HOMO-3)	π (C-C, n)		
7.1	7.23 (HOMO-4)	σ (C-C, C-H)		
-	8.17 (HOMO-5)	σ+π (N-C, C-C)		
9.2	8.78 (HOMO-6)	σ+π (N-C, C-C)		
9.2	9.19 (HOMO-7)	σ (C-C, N-H, C-H)	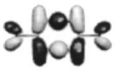	
9.2	9.45 (HOMO-8)	σ (C-C, C-H)	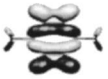	
9.2	9.90 (HOMO-9)	σ (N-C, C-C, N-H, C-H)	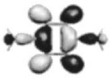	
11.0	11.18 (HOMO-10)	σ (N-H, C-H)	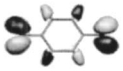	
11.0	11.50 (HOMO-11)	σ (N-C, N-H, C-H)	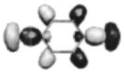	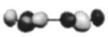
12.0	12.33 (HOMO-12)	σ (N-C, C-H)		
12.0	12.33 (HOMO-13)	σ (N-C, C-C)		

Sketches of the valence molecular orbitals of the *syn*-isomer are depicted in Table I. The side view of the orbital contour allows to determine easily the π or σ character of the orbital. The first four orbitals (HOMO, HOMO-1, HOMO-2 and HOMO-3) are derived from a combination of the π orbitals of benzene and the lone pair of the amine groups. HOMO-4 is the highest occupied σ orbital. HOMO-5 and HOMO-6 are linear combinations of $2p_\sigma$ and $2p_\pi$ atomic orbitals on the carbon and nitrogen atoms and are thus attributed a $\sigma+\pi$ character. The energies of the latter two orbitals are sensitive to the conformation (HOMO-5 =8.2 eV; HOMO-6=8.8 eV for *syn*-PPDA; HOMO-5

TABLE II. Selected structural parameters for PPDA chemisorbed flat (*f*-PPDA) and tilted (*t*-PPDA) on the $Ni_{16}(100)$ model surface. The interatomic distances are in angstroms, and the torsion angle ($\angle$) in degrees. The central atom on the metal surface is noted Ni^*, while the edge-atom involved in the chemisorption is noted Ni.

Bond	C^1N	C^1C^2	C^2C^3	NNi	C^1Ni^*	C^2Ni^*	C^3Ni^*	$\angle H_{phenyl}$	$\angle H_{amine}$
PPDA	1.397	1.393	1.385	⋯	⋯	⋯	⋯	0	30
f-PPDA/Ni_{16}	1.491	1.450	1.479	2.18	1.92	2.30	2.30	28	35
Bond	C^1N	C^1C^2	C^2C^3	C^3C^4	C^4N	NNi^*	C^1Ni^*	$\angle H_{phenyl}$	$\angle H_{amine}$
t-PPDA/Ni_{16}	1.459	1.396	1.395	1.405	1.422	2.10	3.14	0	34

=8.5 eV; HOMO-6=8.6 eV for *anti*-PPDA, see Fig. 2). Towards higher binding energies, all remaining orbitals have σ character.

B. Structure of PPDA chemisorbed on nickel

Figure 3 and Table II collect the main theoretical results. Figure 3 shows the two stable adsorption structures found for PPDA on a Ni(100) surface modeled with a 16-atom nickel cluster. These structures clearly show that chemisorption is taking place. For PPDA adsorbed flat (*f*-PPDA) on the model surface with C_{2v} symmetry, four nickel atoms show distances with the PPDA atoms indicative of the formation of chemical bonds. The shortest distances are to the nitrogen and carbon C^1 atoms: the distance between the nitrogen atoms and the closest nickel atoms is 2.18 Å, and the distance between C^1 and one central nickel atom is 1.92 Å. In Fig. 3, only the four shortest interatomic distances are drawn as bonds for the sake of clarity. However, the distances between the other two carbon atoms and the closest central nickel atoms (2.30 Å) are still smaller than the sum of the van der Waals radii (3.20 Å), thus indicating a covalent character at those interaction sites. The major changes in bond length for PPDA in the adsorbate, relative to the isolated molecule, are significant elongations (between 0.06 Å and 0.09 Å) of all carbon-carbon bonds in the ring, as well as the C–N bonds (0.09 Å). The reason for this geometric rearrangement is the lower availability of the 2*p* electrons of C and N atoms for the π system, because of their involvement in the bonding with the 4*s* and 3*d* electrons of nickel. As a result, the torsion angle defining the position of the hydrogen atoms with respect to the aromatic ring increases from 0° to 28°, which can be interpreted as a change in apparent hybridization of all backbone atoms from sp^2 to sp^3.

Figure 3(b) displays the molecular structure of tilted PPDA (*t*-PPDA) chemisorbed via one nitrogen atom on top of one central nickel atom. The symmetry of *t*-PPDA is σ_v. The aromatic ring of PPDA is tilted by 30° with respect to the surface. The distance between the nitrogen atom and the closest nickel atom is 2.10 Å, which indicates the formation of a chemical bond. The distance between C^1 and the two central nickel atoms (3.14 Å and 3.16 Å) is similar to the sum of the van der Waals radii (3.20 Å). Consequently, PPDA is bound to nickel only via the lone-electronic pair of nitrogen. The major change in bond length for PPDA is a significant elongation (0.06 Å) of the C–N bond when the nitrogen atom interacts with nickel. The new bond is characterized by a $Ni-N-C^1$ angle of about 125°. The other C–N bond is stretched by 0.025 Å. The phenyl ring is much less affected by the adsorption with only a slight elongation of 0.01 Å for the C^2-C^3 and C^3-C^4 bonds; while the C^1-C^2 bond length remains unmodified. The carbon-bonded hydrogen atoms remain in the plane of the phenyl ring. The flat potential surface found for the chemisorption of ethylene on $Ni_{16}(100)$ (the E_{chem} difference between sites is at most 12 kcal/mol) (Ref. 36) and the large chemisorption energy difference found here between *t*-PPDA and *f*-PPDA on $Ni_{16}(100)$ (30 kcal/mol) suggest that the existence of various adsorption sites for PPDA on the surface is not expected to affect the general trend: *f*-PPDA is strongly chemisorbed compared to *t*-PPDA.

C. Charge transfer between PPDA and nickel

Although there are various possible origins for the interface dipoles,[57,58] a significant contribution may arise from the chemical dipole potential D_{chem}.[36] It only appears for chemisorption, i.e., upon occurrence of a significant overlap and rearrangement of the electron densities between the adsorbate and the metal adsorption site. The rearrangement of the electron density on the adsorbate is seen as a partial charge transfer. The formation of chemical bonds accompanied with a partial charge transfer is a well-known chemical concept early described as the Sanderson principle of electronegativity equalization.[59] Nowadays, this phenomenon is fully rationalized in DFT and described with the concept of electronic chemical potential. When two systems (in our case, a metal surface and an organic molecule) come in interaction, their electronic chemical potentials tend to equalize; this determines the direction of electron transfer.[60,61] The electron goes from the species with the higher chemical potential towards that with the lower chemical potential.

The chemical potential μ of a molecule is the derivative of the electronic energy *E* relative to the number of electrons *N* [Eq. (2a)]; in molecules, it can be estimated (from the so-called finite-difference approximation) as the opposite of the average of the first ionization potential (IP) and the electron affinity (EA),[62,63] Eq. (2b) (note that this corresponds to the opposite of Mulliken's expression for electronegativity[64]); for metals, the DFT chemical potential is the opposite of the work function,[65,66] Eq. (2c):

$$\mu = \left(\frac{\partial E}{\partial N}\right)_{v_{ext}}. \tag{2a}$$

$$\text{For molecules:} \quad \mu_A \cong -\frac{\text{IP} + \text{EA}}{2}. \tag{2b}$$

TABLE III. Decrease in Hirshfeld atomic charges (in $|e|$) for PPDA adsorbed flat (*f*-PPDA) and tilted (*t*-PPDA) on the $Ni_{16}(100)$ upon chemisorption. Only carbon and nitrogen atoms are selected because of their relevance for XPS core-level shift contributions. The Hirshfeld total charge q(PPDA) and the dipole moment component perpendicular to the surface $D_{\perp}$, in Debye, are also reported. The dipole moment is calculated for the [PPDA-$Ni_{16}(100)$] system.

Atoms	N^1	C^1	C^2	C^3	C^4	N^2	q(PPDA)	$D_{\perp}$
f-PPDA/Ni_{16}	0.095	0.007	0.025	0.025	0.007	0.095	0.34	6.9
t-PPDA/Ni_{16}	0.107	0.010	0.016	0.008	0.012	0.006	0.20	5.3

For metals: $\mu_m \cong -W$. (2c)

At the DFT level, the derivative in Eq. (2a) is calculated with a constant external potential $v_{\text{ext}}(r)$, equal to the electron-nuclei potential plus any other potential applied to the system. The predicted direction of partial charge transfer upon chemisorption of PPDA on nickel is given by the difference in chemical potentials.[36] The chemical potential of the molecule is evaluated from the calculated IP and EA [Eq. (2b)]: $\mu^{\text{DFT}}(\text{PPDA}) = -2.8$ eV. The high value of the chemical potential of PPDA is the signature of its reducing (i.e., electron-donating) character. Since the experimental chemical potential of a polycrystalline nickel surface [~ -5 eV, Eq. (2c)] and that of the Ni_{16} nickel cluster (~ -4 eV) are lower than μ^{DFT}(PPDA), a partial charge transfer is expected from the PPDA molecule to the nickel surface (experimentally) and the nickel cluster (in the model calculations). This is indeed the case: the chemisorption of PPDA on the nickel cluster is accompanied by a partial charge transfer from the PPDA adsorbate to the metal surface. The Hirsfeld charge q(PPDA) carried by PPDA chemisorbed flat onto the nickel surface ($0.34|e|$) is larger than for *t*-PPDA ($0.20|e|$). This charge transfer creates an electrostatic dipole, the chemical dipole D_{chem}, which is contributing to the total interface dipole at the organic/metal interface. At low PPDA coverage, the charge transfer is expected to be largest for the actual nickel surface, because of its lower chemical potential and its smaller hardness,[18] compared to the nickel cluster.

The atomic charge distribution (Table III) reveals that PPDA chemisorbed parallel to the surface displays a strong decrease in electronic density on the nitrogen atoms: 70% of the transferred charge is originating from the two amine groups. The remaining partial positive charge is delocalized on the phenyl ring, especially around the C^2-C^3 bonds. For *t*-PPDA, 56% of the positive charge is on the amine group in contact with the nickel surface. Note that there is still significant delocalization of the charge on the aromatic ring, as well as on the other amine group.

The theoretical investigation shows that strong dipole moments result from the chemisorption of PPDA on nickel. The positive pole of the dipole is on the molecule, while the negative side is on the metal surface. The calculated dipole moment for the entire [PPDA-$Ni_{16}(100)$] complex has a large component $D_{\perp}$ perpendicular to the metal surface: 6.9 D for *f*-PPDA and 5.3 D for *t*-PPDA. The high symmetry of PPDA leads to a small permanent dipole moment in the syn-conformation [1.1*D* (Ref. 52)]. Hence, the large calculated dipoles are believed to be mainly due to the modification of the metal electron density at the surface in combination with the partial charge transfer upon chemisorption. The two phenomena cannot be separated, but their contributions change the interface dipole in the same direction. Consequently, strong dipoles created at the PPDA/Ni interface are expected to result in a decrease of the work function of nickel.

D. Chemisorption as mixing of molecular orbitals

Figure 4 displays a comparison between the LDOS of PPDA in [*t*-PPDA-Ni_{16}] complex (spectrum *a*), [*f*-PPDA-Ni_{16}] (spectrum *c*) and the total DOS of the isolated PPDA molecule (spectrum *b*). The HOMO of the [PPDA-Ni_{16}] complexes is mostly localized on the metal cluster. Since the complexes possess a tiny HOMO-LUMO gap (0.003 eV), the HOMO energy is associated to the chemical potential μ[PPDA-Ni_{16}] defined in Eq. (2a). Note that the comparison between the LDOS spectra (using calculated eigenenergies) and UPS spectra is only qualitative for several reasons: (i) the chemical potential of the nickel cluster $\mu[Ni_{16}]$ (-4.0 eV) is higher than for the actual metal ($\mu = -W = -5.1$ eV); (ii) spectroscopy data include significant final state effects when photoemission occurs from an adsorbate at the vicinity of a metal surface; (iii) photoelectron emission cross-sections are not taken into account when computing LDOS.

The *t*-PPDA adsorbate interacts mainly with the nickel surface via one nitrogen atom. The π orbitals localized on the phenyl ring, such as HOMO-1 and HOMO-4 (Table I), are only weakly coupled to the surface and appear almost unchanged upon chemisorption (compare peaks $2 \rightarrow t2$, $4 \rightarrow t5$). π orbitals with a significant weight on the nitrogen atom, such as HOMO (peak 1) and HOMO-2 (peak 3), interact with the 3*d*-4*s* orbitals of nickel and appear as peaks *t*1 and *t*3 in the LDOS spectrum of [*t*-PPDA-Ni_{16}]. Since the overlap between those molecular orbitals and the metal wave function occurs only via the nitrogen atom, the modification of the shape of the peaks in the LDOS is small. However, due to the partial charge transfer from PPDA to Ni_{16}, those two peaks appear shifted by 0.6 eV towards higher binding energies. Interestingly, the energy shift of occupied and unoccupied orbitals is not symmetric. The LUMO level of PPDA (-2.2 eV) is not only broadened in [*t*-PPDA-Ni_{16}], but also significantly shifted (1.8 eV). Note that the complex has a nonzero LDOS on PPDA at its chemical potential.

When PPDA is chemisorbed flat on the surface, all π orbitals overlap with the 3*d*-4*s* band of nickel. The overlap is significant, since it occurs via several atomic sites of the phenyl ring and the amine groups. This results in a complete damping of peaks in the LDOS spectrum. Peaks 1, 2, and 3 of PPDA are in the energy range of the 3*d*-4*s* levels of nickel; their overlap with the metal wave function gives rise to the creation of many orbitals, delocalized between PPDA

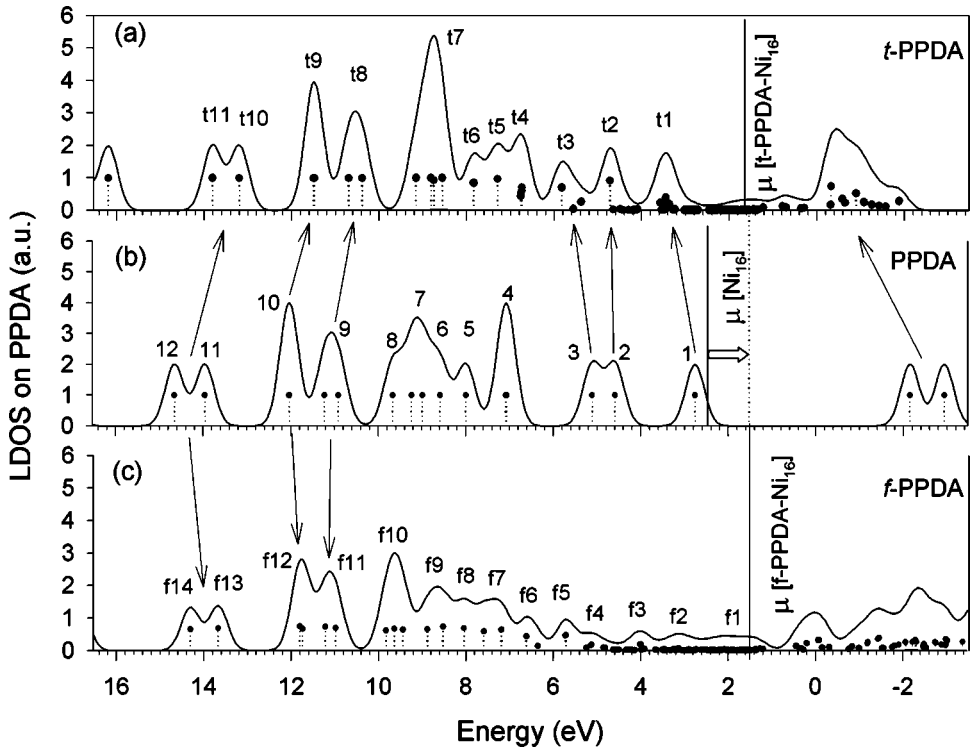

FIG. 4. Local-density-of-states spectra of PPDA (LDOS) in the [*f*-PPDA-Ni_{16}] and [*t*-PPDA-Ni_{16}] complexes are compared to the total density of states of an isolated PPDA molecule. The total density of states of an isolated PPDA molecule (curve *b*) is in good agreement with the UPS spectrum of a PPDA multilayer (Fig. 2). The eigenenergy of the orbitals in the model systems have been rigidly shifted so that the HOMO of the isolated PPDA molecule corresponds to the ionization potential of the multilayer. Consequently, the zero energy thus corresponds to the Fermi level in the UPS of a PPDA multilayer. The graph also shows the chemical potential for Ni_{16}, as well as those for [*f*-PPDA-Ni_{16}] and [*t*-PPDA-Ni_{16}] complexes.

and the metal cluster. This is visualized as a complete spread of the three peaks into wide bands (*f*1, *f*2, *f*3, and *f*4) up to the chemical potential of the complex.

For both types of adsorbates, *t*-PPDA or *f*-PPDA, the unoccupied levels are strongly shifted (by ~2 eV) to lower binding energies. Moreover, the chemical potential of the nickel cluster $\mu(Ni_{16})$ (which is related to the Fermi level of the actual surface) is increased by 0.7 eV upon PPDA chemisorption. This again is associated to the electron density flow from PPDA to the nickel cluster, which becomes negatively charged after chemisorption. This suggests that one monolayer of electron donor molecules can lead to a significant reduction of the electron injection barrier compared to the value estimated simply as the difference between the LUMO and the Fermi level of the isolated components (PPDA and the nickel surface, respectively).

V. EXPERIMENTAL RESULTS

A. Early stage of formation of a PPDA mono-layer

Upon deposition of PPDA at −40 °C (above the condensation temperature to avoid multilayer formation), the work function decreases rapidly by 1.55 eV reaching 3.55 eV (Fig. 5). The measured work function decrease for PPDA is significantly larger than the work function decrease obtained with a full coverage of a physisorbed Xe monolayer on nickel [0.8 eV (Refs. 4 and 36)]. The larger work function decrease observed with PPDA is likely due to molecular chemisorption, more specifically, to the partial charge transfer from the molecule to the metal and the creation of a chemical dipole D_{chem}.

The evolution of the UPS spectra versus the deposition time *t* is shown in Fig. 6. Only some UPS spectra are shown for specific deposition time; their label corresponds to those in Fig. 5. Starting from atomically clean nickel (a) with an intense signal about 1 eV related to its 3*d* band, the deposition of PPDA at low coverage (b) is accompanied by the appearance of a broad photoelectron emission with four shoulders about 5 eV, 6 eV, 8 eV, and 11 eV. The XPS

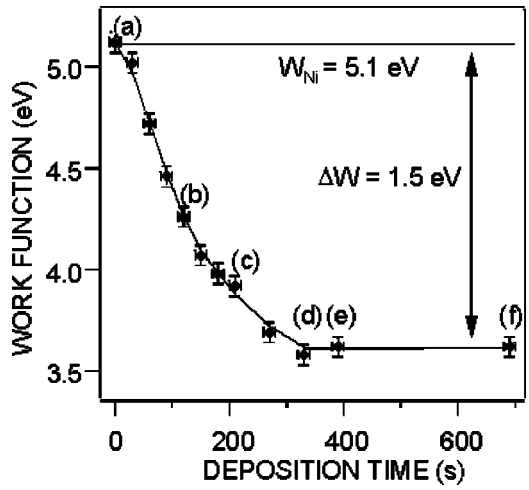

FIG. 5. Nickel work function vs PPDA deposition time at $T=-40$ °C (above the condensation temperature).

N(1*s*) signal of the submonolayer is displayed in Fig. 7 for various stages of the monolayer formation. The N(1*s*) signal (b) is composed of two peaks of similar intensity at 397.9 eV and 400.1 eV. At low surface coverage, the presence of these two N(1*s*) contributions indicates that the two nitrogen atoms of PPDA, which are obviously equivalent in the gas phase, have different environments when the molecules are chemisorbed. The nitrogen atoms chemically bound to the metal appear at a lower binding energy, because of the metal-screening effect. The second type of nitrogen atom is further away from the metal surface and most probably corresponds to N^2 in the *t*-PPDA model [Fig. 3(b)]. Indeed the component at 400.1 eV has the same binding energy as the single N(1*s*) peak of the multilayer (see Fig. 8). A significant screening contribution of the core hole created upon photoemission arises from the metal surface. The screening energy estimated from the Jones–Jennings–Jepsen (JJJ) potential for nickel,[67,68] reaches about 2.3 eV (Refs. 17 and 36) for the $Ni-N^1$ interatomic distance of about 2 Å, as obtained from the model system *t*-PPDA-Ni_{16} and *f*-PPDA-Ni_{16} (see Table II); while it is about 0.5 eV for N^2 atoms, which are distant by 5.1 Å from the surface nickel atoms. The metal screening for atoms in direct contact with the metal overwhelms other effects, such as the decrease in electron density around the chemically bound nitrogen atoms (Table III). Note that N(1*s*) component of the N^1 atom in *t*-PPDA is expected to have lower intensity compared to that of N^2 because photoelectrons emitted from N^1 are inelastically scattered by the electron density of the molecule itself that is tilted by 30° on the surface. At this low PPDA coverage, the equal intensity of the high and low energy N(1*s*) features suggests that the first stage of monolayer formation is the chemisorption of PPDA molecules both chemisorbed tilted *t*-PPDA and flat *f*-PPDA on the surface. The UPS spectrum at this low coverage is poorly defined. Note that the contribution from *f*-PPDA is likely difficult to observe since the theoretical LDOS spectrum of *f*-PPDA is very broad due to the strong electronic coupling with the metal (Fig. 4). Despite the low coverage, the work function decreases significantly from 5.1 eV, for the sputter-cleaned nickel surface, to 4.2 eV, for the PPDA submonolayer [Fig. 5(b)]. This is attributed to the creation of chemical dipoles resulting from a partial electron transfer from PPDA to nickel upon chemisorption of *t*-PPDA and *f*-PPDA.

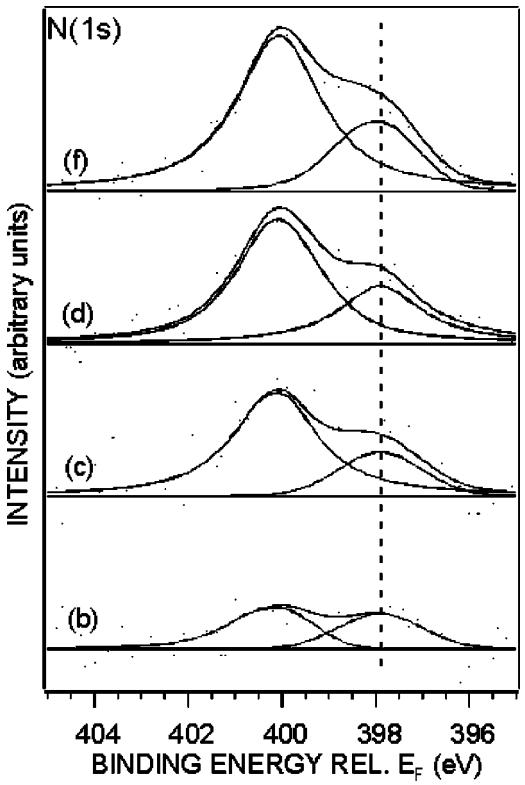

FIG. 7. Evolution of the XPS N(1*s*) signal upon PPDA deposition on nickel. The labeling corresponds to that in Fig. 5(a). Valence levels of the cleaned nickel surface, (b) first stage of formation of PPDA monolayer, (c–f) second stage of formation of the monolayer. The binding energy (eV) is relative to the Fermi level.

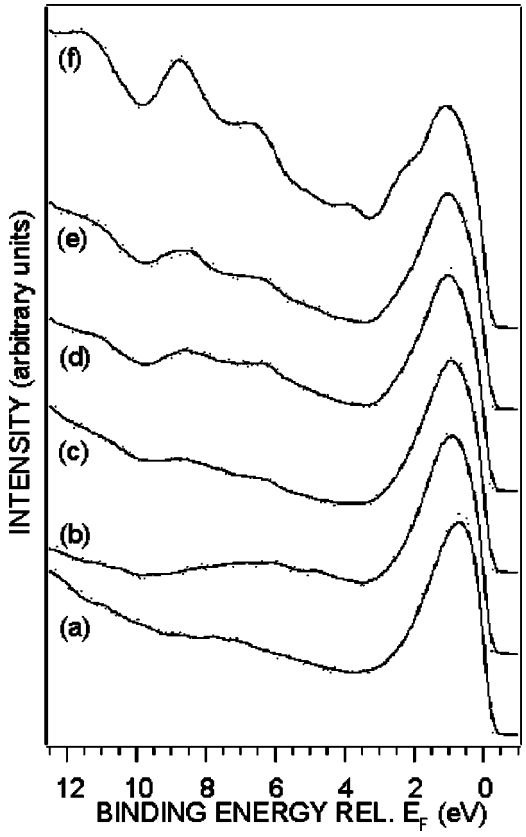

FIG. 6. Evolution of the UPS spectra recorded upon PPDA deposition on nickel: (a) Valence levels of the cleaned nickel surface, (b) first stage of formation of PPDA monolayer, (c–f) second stage. The binding energy (eV) is relative to the Fermi level.

B. Characterization of the saturated PPDA monolayer

After the first stage of formation of the monolayer, the UPS spectra [from spectrum (b)–(f) in Fig. 6] start to display well-defined peaks increasing in intensity upon deposition time. Simultaneously, the high energy component of the N(1*s*) spectra (Fig. 7), associated to the N^2 atom of *t*-PPDA, is enhanced. It can thus be concluded that the second stage of monolayer formation corresponds to the occupation of nickel adsorption sites by PPDA molecules in a tilted conformation. In agreement with the UPS spectra, *t*-PPDA has a well-

defined valence structure as compared to *f*-PPDA because of the weaker electronic coupling with the metal surface (Fig. 4).

The saturation of the work function occurs before the monolayer has fully formed. Subsequent deposition steps are still accompanied by a decrease of the nickel 3*d*-band emission while the valence levels of the organic monolayer become clearly visible. The UPS spectrum of the saturated PPDA monolayer at −40 °C (curve *f*, Fig. 6) shows four peaks at 11.5, 9.0, 6.8, 4.1 eV. and one shoulder at about 2.4 eV close to the 3*d* band of nickel (at about 1 eV, see spectrum *e*). The small intensity of the Ni signal as compared with the valence features of PPDA indicates that the chemisorbed monolayer is densely packed at −40 °C. The valence features of the saturated monolayer correspond to those of a PPDA multilayer (Fig. 2) or PPDA in gas phase.[53] This indicates that most of the molecules at the surface are PPDA molecularly chemisorbed, not cleaved, with their molecular orbitals weakly modified upon chemisorption; those corresponds to *t*-PPDA adsorbates.

C. Stability of the PPDA monolayer upon annealing

Figure 8 shows the evolution of the N(1*s*) and C(1*s*) signals for PPDA molecules deposited on a clean, polycrystalline nickel surface upon increasing the substrate temperature from −85 °C to 200 °C. The starting point corresponds to a PPDA multilayer (−85 °C) characterized by one symmetric N(1*s*) peak at 400.1 eV. This peak contains the signal of the two chemically equivalent nitrogen atoms of PPDA. The C(1*s*) line shape displays two peaks; at 285.1 eV and 286.1 eV with a 2:1 intensity ratio. The low binding energy peak is due to the four carbon atoms of the center of the aromatic ring, while the high binding energy component is attributed to the two carbon atoms that are slightly electron deficient due to their chemical bond with the amine groups.

When the temperature is raised to −35 °C i.e., above the desorption temperature for multilayers, the N(1*s*) and C(1*s*) peaks decrease but remain clearly visible and very similar to the signal coming from the monolayer formed at −40 °C in the preceding section. Some PPDA molecules do not desorb because they interact strongly with the nickel surface, and form the densely packed chemisorbed monolayer. An additional feature of the chemisorption is the second N(1*s*) peak that appears at 398.2 eV, i.e., 1.9 eV shifted towards lower binding energy with respect to the signal of the multilayer, as well as a modification of the C(1*s*) line shape. The origin of the two components in the N(1*s*) signal has been discussed above.

The overall C(1*s*) and N(1*s*) spectral intensities for the monolayer are proportional to the surface coverage. From −35 °C to 50 °C, both XPS signals decrease; moreover, the 3*d* band of nickel becomes more visible in the UPS spectra (Fig. 9) compared to the molecular features. The N(1*s*) component at 400 eV coming from *t*-PPDA diminishes while the low energy component is enhanced. Those observations suggest that the molecular desorption of some *t*-PPDA adsorbates is taking place, together with the beginning of the dehydrogenation of *t*-PPDA molecules.

In order to shed light on the relationship between the two

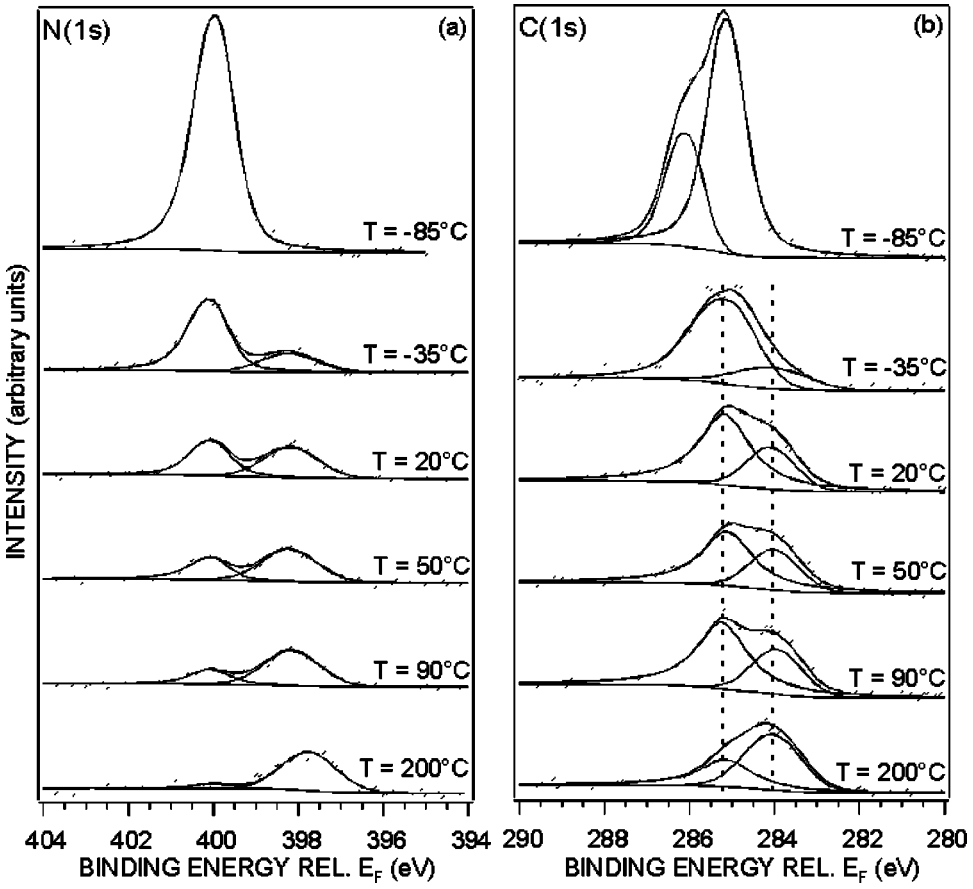

FIG. 8. Evolution of the (a) N(1*s*) and (b) C(1*s*) signals of a PPDA multilayer upon increasing the temperature from −85 °C to +200 °C. The binding energy is relative to the Fermi level. The deconvolution of the C(1*s*) monolayer spectra obtained at various temperature is realized with the following constraints: the shape of the two peaks is kept constant, as well as their binding energy difference. Note that the two peaks do not correspond to the two types of C in the multilayer film of PPDA.

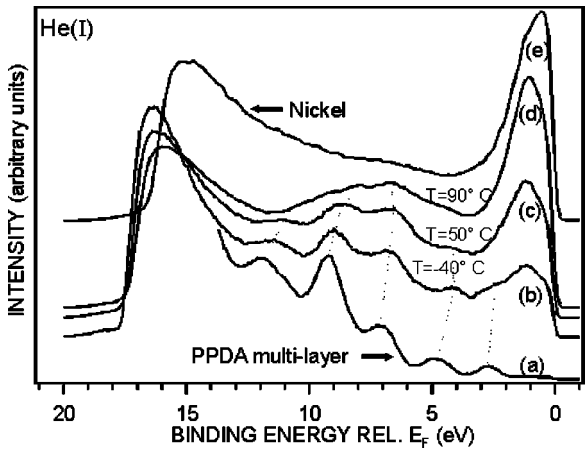

FIG. 9. Comparison between the UPS He(I) spectra of (a) a PPDA multilayer, a PPDA monolayer at various temperatures: −40 °C (b), 50 °C (c), and 90 °C (d); and, a clean nickel surface (e). Binding energies, in eV, are relative to the Fermi level.

contributions in the N(1*s*) and C(1*s*) spectra and the molecular orientations, the geometry of the experiment is changed. The PPDA monolayer persisting at room temperature is characterized by N(1*s*) and C(1*s*) spectra recorded at two different electron-emission angles, $\theta=0°$ and $\theta=60°$ defined with respect to the surface normal (Fig. 10). Collecting the photoelectrons at grazing angle strongly increases the surface sensitivity of the experiment. When the sample is tilted at $\theta=60°$, the high energy contributions N(1*s*) (400.1 eV) and C(1*s*) (285.5 eV) are increased. Those signals are therefore attributed to nitrogen and carbon atoms at the very surface of the monolayer, which do not interact directly with the nickel surface and are thus not yet involved in the dehydrogenation process. The low binding energy contributions are related to atoms close to the metal surface, some being covalently bound to nickel, which are thus activated for the dehydrogenation reaction.

Temperature-programmed reaction studies showed the molecular desorption of aniline chemisorbed on the (100) nickel surface between 0 °C and 100 °C, followed by dehydrogenation reactions between 20 °C and 420 °C. Upon heating, dehydrogenation of aniline is characterized by a new N(1*s*) component at 397.2 eV and a new low energy component on the C(1*s*) spectrum.[26] Similar spectral modifications are visible in Fig. 8 for PPDA chemisorbed on nickel upon annealing. Between 90 °C and 200 °C, the spectral line shapes are strongly modified. As the temperature is gradually raised, the component at 398.2 eV in the N(1*s*) spectrum grows while the peak at 400 eV tends to disappear. Simultaneously, the C(1*s*) line shape shows similar trends with a loss of intensity in the high binding energy region (about 285 eV) and an increase of the signal at about 284 eV. A tentative explanation is that upon dehydrogenation of the N^1H_2 amine group of *t*-PPDA, the phenyl ring may be forced to be parallel to the surface, thus making the second N^2H_2 amine group in contact with nickel and thus activated for further dehydrogenation. The proximity of the phenyl ring to the metal is indicated by the growth of the low binding energy in the C(1*s*) spectra. The cleavage and/or strong electronic coupling of the phenyl ring are consistent with the systematic loss of resolution in the UPS spectra upon heating (Fig. 9). At 90 °C, the valence levels from the molecules are so broad that they merge in a large bump spread between 3 eV and 12 eV. The metal coverage is much lower, 24% of the maximum coverage, as estimated by the lower signal intensity in the N(1*s*) spectrum and indicated by the intense metal contribution at 1 eV emerging in the UPS spectrum. Interestingly, despite this low coverage, the work function remains low (3.8 eV). Upon annealing, a surface coverage decrease by 76% is therefore accompanied by an increase of only 0.25 eV in work function. Apparently, a low coverage of PPDA molecules chemisorbed or dehydrogenated on nickel is enough to decrease the metal work function significantly by 1.3 eV.

VI. SUMMARY AND CONCLUSIONS

Photoelectron spectroscopies and density functional theory calculations are used to investigate the interaction between *para*-phenylenediamine, an electron donor, and a polycrystalline nickel surface. Theoretical models show that PPDA chemisorbs on the model Ni(100) surface in two possible conformations: either PPDA is tilted on the surface (with the phenyl ring at 30° from the surface plane) and interacts via one of its nitrogen lone pair; or PPDA is chemisorbed flat on the surface (*f*-PPDA) bond to the surface via C–Ni and N–Ni bonds. The theoretical results are in good agreement with the spectroscopic data characterizing the

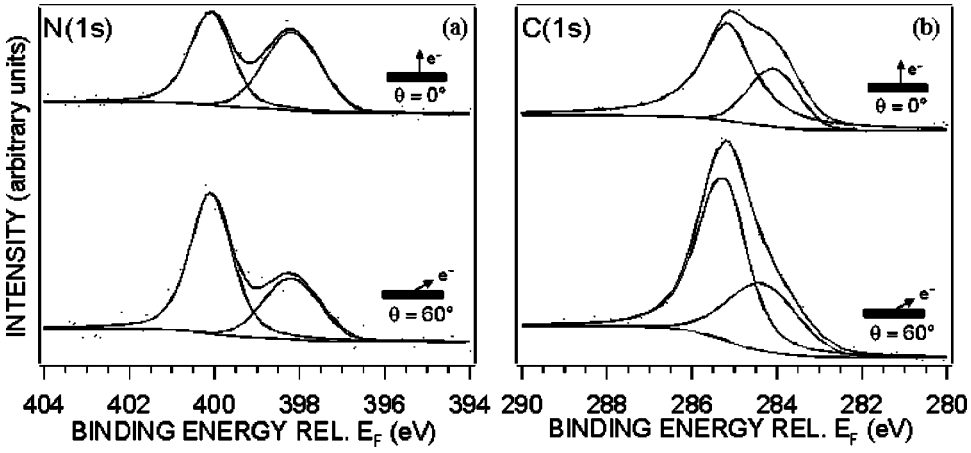

FIG. 10. N(1*s*) and C(1*s*) spectra of a PPDA monolayer chemisorbed on a polycrystalline nickel surface at 20 °C for two different emission angles θ of the photoelectrons: normal to the surface ($\theta=0°$) and at grazing angle ($\theta=60°$). Binding energies, in eV, are relative to the Fermi level.

PPDA monolayer formation on a nickel surface cooled down to −40 °C. At this temperature, gaseous PPDA molecules approaching the surface are trapped mostly in the flat conformation. Theoretical models predict this conformation to have higher chemisorption energy by about 30 kcal/mol. This is both supported by the UPS and XPS data. UPS shows a significant broadening of the molecular features in good agreement with theoretical model for *f*-PPDA. Note that the titled conformation coexists to some extent due to the low temperature. At higher surface coverage, free nickel adsorption sites are occupied by the tilted conformation as evidenced by clear molecular features emerging in the UPS spectra and the increase of the N(1*s*) signal at 400 eV.

In both conformations, the equalization of the electronic chemical potentials between PPDA and the surface model predicts a partial electron transfer from PPDA, the electron donor, to the nickel surface atoms upon chemisorption. This charge redistribution creates a chemical dipole that contributes, together with the modification of the electronic density at the metal surface, to the overall interface dipole when a monolayer is chemisorbed on nickel. The interface dipole formed upon chemisorption of one PPDA monolayer changes the work function of the polycrystalline nickel from 5.10 eV to 3.55 eV. Those results indicate that the chemisorption of a donor molecule on a metal electrode is a possible alternative to improve the electron injection from a metal to an organic semiconductor.

Annealing the monolayer leads to dehydrogenation reactions of PPDA activated by the interaction with the nickel surface. Dehydrogenation occurs from 20 °C up to 200 °C. This is evidenced by the large changes in the N(1*s*) and C(1*s*) core-level spectra of PPDA, as well as by the loss of molecular features in the valence levels spectrum. Upon dehydrogenation of the N^1H_2 amine group of *t*-PPDA, the phenyl ring may be forced to be parallel to the surface, thus bringing the second N^2H_2 amine group in contact with nickel and activating further dehydrogenation.

ACKNOWLEDGMENTS

Research in Norrköping and Linköping was supported by the Swedish Foundation for Strategic Research (SSF) through the Project COE and by the Swedish Science Research Council (VR). M.P.deJ. was supported in Linköping by the Center of Advanced Molecular Materials (CAMM), also funded by SSF. The Mons–Linköping collaboration is supported by the European Commission, within the 6th Framework of the European Commission, in an Integrated Project, NAIMO (NMP4-CT2004-500355).

[1] P. K. H. Ho, J.-S. Kim, J. H. Burroughes, H. Becker, S. F. Y. Li, T. M. Brown, F. Cacialli, and R. Friend, Nature (London) **404**, 481 (2000).
[2] A. Vilan, A. Shanzer, and D. Cahen, Nature (London) **404**, 166 (2000).
[3] *Conjugated Polymer and Molecular Interfaces: Science and Technology for Photonic and Optoelectronic Applications*, edited by W. R. Salaneck, K. Seki, A. Kahn, and J.-J. Pireaux (Marcel Dekker, New York, 2002).
[4] Y. C. Chen, J. E. Cunningham, and C. P. Flynn, Phys. Rev. B **30**, 7317 (1984).
[5] M. A. Baldo and S. R. Forrest, Phys. Rev. B **64**, 085201 (2001).
[6] J. C. Scott, J. Vac. Sci. Technol. A **21**, 521 (2003).
[7] E. Ito, H. Oji, N. Hayashi, H. Ishii, Y. Ouchi, and K. Seki, Appl. Surf. Sci. **175–176**, 407 (2001).
[8] H. Ishii and K. Seki, IEEE Trans. Electron Devices **44**, 1295 (1997).
[9] H. Ishii, K. Sugiyama, E. Ito, and K. Seki, Adv. Mater. (Weinheim, Ger.) **11**, 605 (1999).
[10] I. G. Hill, A. Rajagopal, A. Kahn, and Y. Hu, Appl. Phys. Lett. **73**, 662 (1998).
[11] J. Blochwitz, T. Fritz, M. Pfeiffer, K. Leo, D. M. Alloway, P. A. Lee, and N. R. Armstrong, Org. Electron. **2**, 97 (2001).
[12] D. Schlettwein, K. Hesse, N. E. Gruhn, P. A. Lee, K. W. Nebesny, and N. R. Armstrong, J. Phys. Chem. B **105**, 4791 (2001).
[13] X. Crispin, V. M. Geskin, A. Crispin, J. Cornil, R. Lazzaroni, W. R. Salaneck, and J. L. Brédas, J. Am. Chem. Soc. **124**, 8132 (2002).
[14] L. Yan, N. J. Watkins, S. Zorba, Y. Gao, and C. W. Tang, Appl. Phys. Lett. **81**, 2752 (2002).
[15] P. S. Bagus, V. Staemmler, and C. Wöll, Phys. Rev. Lett. **89**, 096104 (2002).
[16] N. D. Lang, Phys. Rev. B **4**, 4234 (1971).
[17] X. Crispin, R. Lazzaroni, A. Crispin, V. M. Geskin, J. L. Brédas, and W. R. Salaneck, J. Electron Spectrosc. Relat. Phenom. **121**, 57 (2001).
[18] X. Crispin, V. Geskin, R. Lazzaroni, C. Bureau, W. Salaneck, and J. L. Brédas, J. Chem. Phys. **111**, 3237 (1999).
[19] I. H. Campbell, J. D. Kress, R. L. Martin, D. L. Smith, N. N. Barashkov, and J. P. Ferraris, Appl. Phys. Lett. **71**, 3528 (1997).
[20] R. W. Zehner, B. F. Parsons, R. P. Hsung, and L. R. Sita, Langmuir **15**, 1121 (1999).
[21] J. Krüger, U. Bach, and M. Grätzel, Adv. Mater. (Weinheim, Ger.) **12**, 447 (2000).
[22] A. Vilan, A. Shanzer, and D. Cahen, Nature (London) **404**, 166 (2000).
[23] J. E. Whitten, Surf. Sci. **546**, 107 (2003).
[24] D. E. Gardin and G. A. Somorjai, J. Phys. Chem. **96**, 9424 (1992).
[25] S. X. Huang, D. A. Fischer, and J. L. Gland, J. Phys. Chem. **100**, 13629 (1996).
[26] S. X. Huang, D. A. Fisher, and J. L. Gland, J. Phys. Chem. **100**, 10223 (1996).
[27] S. X. Huang and J. L. Gland, J. Phys. Chem. **100**, 2206 (1996).
[28] Scienta, Scienta ESCA 200 Users' Manual (Uppsala).
[29] S. Trasatti, Electrochim. Acta **37**, 2137 (1992).
[30] G. te Velde and E. J. Baerends, Chem. Phys. **177**, 399 (1993).
[31] K. Hermann, P. S. Bagus, and C. J. Nelin, Phys. Rev. B **35**, 9467 (1987).
[32] C. Mijoule, M. F. Baba, and V. Russier, J. Mol. Catal. **83**, 367 (1993).
[33] I. Panas, J. Schüle, P. Siegbahn, and U. Wahlgren, Chem. Phys. Lett. **149**, 265 (1988).
[34] X. Crispin, V. Geskin, R. Lazzaroni, C. Bureau, and J. L. Brédas, Eur. J. Inorg. Chem. **1999**, 349.
[35] K. Horn, A. M. Bradshaw, and K. Jacobi, J. Vac. Sci. Technol. **15**, 575 (1978).
[36] X. Crispin, V. Geskin, A. Crispin, J. Cornil, R. Lazzaroni, W. Salaneck, and J.-L. Brédas, J. Am. Chem. Soc. **124**, 8131 (2002).
[37] R. G. Parr and W. Yang, *Density-Functional Theory of Atoms and Molecules* (Oxford University Press, New York, 1989).
[38] B. Delley, J. Chem. Phys. **92**, 508 (1990).
[39] B. Delley, New J. Chem. **16**, 1103 (1992).
[40] J. Baker, J. Comput. Chem. **7**, 385 (1986).
[41] D. Becke, Phys. Rev. A **38**, 3098 (1988).
[42] J. P. Perdew and Y. Wang, Phys. Rev. B **45**, 13244 (1992).
[43] J. Baker and W. J. Hehre, J. Comput. Chem. **12**, 606 (1991).
[44] J. Baker, J. Comput. Chem. **14**, 1085 (1993).
[45] X. Crispin, R. Lazzaroni, V. Geskin, N. Baute, P. Dubois, R. Jérôme, and J. L. Brédas, J. Am. Chem. Soc. **121**, 176 (1999).
[46] T. Ziegler, Chem. Rev. (Washington, D.C.) **91**, 651 (1991).
[47] F. L. Hirshfeld, Theor. Chim. Acta **44**, 129 (1977).
[48] R. F. Nalewajski and R. G. Parr, J. Phys. Chem. A **105**, 7391 (2001).
[49] P. O. Löwdin, J. Chem. Phys. **18**, 365 (1950).
[50] A. D. Rabuck and G. E. Scuseria, J. Chem. Phys. **110**, 695 (1999).
[51] J. Cornil, S. Vanderdonckt, R. Lazzaroni *et al.*, Chem. Mater. **11**, 2436 (1999).
[52] Y. Y. Borovikov, V. P. Makovetskii and N. S. Pivovarova, Ber. Bunsenges. Phys. Chem. **100**, 33 (1996).
[53] M. H. Palmer, W. Moyes, M. Spiers, and J. N. A. Ridyard, J. Mol. Struct. **53**, 235 (1979).
[54] W. Salaneck, Phys. Rev. Lett. **40**, 60 (1978).
[55] N. Sato, K. Seki, and H. Inokuchi, J. Chem. Soc., Faraday Trans. 2 **77**, 1621 (1981).

[56]N. Sato, H. Inokuchi, and I. Shirotani, Chem. Phys. **60**, 327 (1981).
[57]H. Ishii, K. Sugiyama, E. Ito, and K. Seki, Adv. Mater. (Weinheim, Ger.) **11**, 605 (1999).
[58]L. Yan, N. J. Watkins, S. Zorba, Y. Gao, and C. W. Tang, Appl. Phys. Lett. **81**, 2752 (2002).
[59]R. T. Sanderson, Science **114**, 670 (1951).
[60]R. F. Nalewajski, J. Am. Chem. Soc. **106**, 944 (1984).
[61]W. J. Mortier, S. K. Ghosh, and S. Shankar, J. Am. Chem. Soc. **108**, 4315 (1986).
[62]R. G. Parr, R. A. Donnelly, M. Levy, and W. E. Palke, J. Chem. Phys. **68**, 3801 (1978).
[63]R. G. Parr and R. G. Pearson, J. Am. Chem. Soc. **105**, 7512 (1983).
[64]R. S. Mulliken, J. Chem. Phys. **2**, 782 (1934).
[65]N. D. Lang and W. Kohn, Phys. Rev. B **3**, 1215 (1970).
[66]F. Garcia-Moliner and F. Flores, *Introduction to The Theory of Solid Surfaces* (Cambridge University Press, Cambridge, 1979).
[67]R. O. Jones, P. J. Jennings, and O. Jepsen, Phys. Rev. B **29**, 6474 (1984).
[68]N. V. Smith, C. T. Chen, and M. Weinert, Phys. Rev. B **40**, 7565 (1989).